

Local Jet Pattern: A Robust Descriptor for Texture Classification

Swalpa Kumar Roy[†], *Student Member, IEEE*, Bhabatosh Chanda, Bidyut B. Chaudhuri, *Life Fellow, IEEE*, Soumitro Banerjee, *Fellow, IEEE*, Dipak Kumar Ghosh and Shiv Ram Dubey, *Member, IEEE*

Abstract—Methods based on local image features have recently shown promise for texture classification tasks, especially in the presence of large intra-class variation due to illumination, scale, and viewpoint changes. Inspired by the theories of image structure analysis, this paper presents a simple, efficient, yet robust descriptor namely local jet pattern (LJP) for texture classification. In this approach, a jet space representation of a texture image is derived from a set of derivatives of Gaussian (DtGs) filter responses up to second order, so called local jet vectors (LJV), which also satisfy the Scale Space properties. The LJP is obtained by utilizing the relationship of center pixel with the local neighborhood information in jet space. Finally, the feature vector of a texture region is formed by concatenating the histogram of LJP for all elements of LJV. All DtGs responses up to second order together preserves the intrinsic local image structure, and achieves invariance to scale, rotation, and reflection. This allows us to develop a texture classification framework which is discriminative and robust. Extensive experiments on five standard texture image databases, employing nearest subspace classifier (NSC), the proposed descriptor achieves 100%, 99.92%, 99.75%, 99.16%, and 99.65% accuracy for Outex_TC-00010 (Outex_TC10), and Outex_TC-00012 (Outex_TC12), KTH-TIPS, Brodatz, CURET, respectively, which are outperforms the state-of-the-art methods.

Index Terms—Derivative-of-Gaussian (DtGs) Filter, Image derivatives, Local binary pattern (LBP), Local jet vector (LJV), Local jet Pattern (LJP), Scale invariance, Jet space, Scale space, Texture classification.

I. INTRODUCTION

TEXTURE is a fundamental characteristic of appearance of virtually all natural surfaces and is ubiquitous in natural images. Texture classification is one of the major problems in texture analysis and has received a lot of attention during the past decades due to its value in understanding how the texture recognition process works in humans. It also plays a significant role in the field of computer vision and

pattern recognition [1]. A crucial issue of texture analysis is to construct the effective texture representations, belonging to five categories of methodology, such as statistical, geometrical, structural, model-based, and signal processing based [2], [3].

A picture may be captured under various geometric and photometric varying conditions, therefore an ideal model for describing and recognizing textures should be able to capture essential perceptual properties of the texture structure. It should be robust enough against the environmental changes, such as changes in view-point, illuminance, rotation, reflection, scale, and geometry of the underlying surface. Attention has been focussed on the design of local texture descriptors capable of achieving local invariance [4]–[7] and the search for invariances started in the nineties of last century [8]. Kashyap and Khotanzad first proposed a circular autoregressive dense model [9] to study the rotation invariant texture classification. Many other models were explored to study rotation invariance including multi-resolution [10], hidden Markov model [11], and Gaussian Markov model [12]. Recently Varma and Zisserman [6] proposed to learn a rotation invariant texton dictionary from a training set, and then classify the texture image based on its texton distribution. Later on, Varma and Zisserman [7] proposed another texton based algorithm by using the image local patch to represent the feature directly. Some works are recently proposed for scale and affine invariant feature extraction for texture classification. Chaudhuri and Sarkar proposed a technique for texture recognition based on differential box-counting (DBC) [13] based algorithm. Varma and Garg [14] extracted a local fractal vector for each pixel, and computed a statistical histogram; Liu and Fieguth [15] applied random projection for densely sampled image patches, and extracted the histogram signature; Yao and Sun [16] normalized statistical edge feature distribution to resist variation in scale; Lazebnik *et al.* [17] and Zhang *et al.* [4] detected Harris and Laplacian regions and extracted texture signatures after normalizing these regions. Recently, global scale invariant feature extraction methods drew attention because local scale normalization is usually slow due to pixel by pixel operations. Xu *et al.* [18] and Quan *et al.* [19] have classified the image pixels into multiple point sets by gray intensities or local feature descriptors. Other than extracting scale invariant features, pyramid histograms with shifting matching [5] scheme were also proposed by some researchers [20].

In order to impart more robustness, feature extraction is often performed locally. In 1996 a computationally efficient texture descriptor, called local binary pattern (LBP) was proposed by Ojala *et al.* [21], [22] for gray-scale and rotation

S. K. Roy and B. Chanda are with the Electronics and Communication Sciences Unit at Indian Statistical Institute, Kolkata 700108, India (email: swalpa@ieee.org; chanda@isical.ac.in).

B. B. Chaudhuri is with the Computer Vision and Pattern Recognition Unit at Indian Statistical Institute, Kolkata 700108, India (email: bbc@isical.ac.in).

S. Banerjee is with the Department of Physical Sciences at Indian Institute of Science Education and Research, Kolkata, Mohanpur Campus, 741246, India (email: soumitro@iiserkol.ac.in).

D. K. Ghosh is with the Department of Electronics & Communication Engineering at National Institute of Technology, Rourkela, Orissa 769008, India (email: dipak@ieee.org).

S. R. Dubey is with the Department of Computer Science & Engineering at Indian Institute of Information Technology, Sririty 517646, India (email: srdubey@iiits.in).

* Corresponding author email: swalpa@students.iiests.ac.in, swalpa@ieee.org.

invariant texture classification. Later on, other variants of LBP such as center-symmetric LBP (CSLBP) [23], derivative-based LBP [24], LBP variance (LBPV) [25], the dominant LBP (DLBP) [26], the completed model of LBP (CLBP) [27], order-based local descriptor [28], local wavelet pattern [29], and multichannel decoded LBP [30] etc. were introduced in numerous applications of computer vision and pattern recognition. But these methods could not address the scaling issue very well and LBP feature alone could not achieve good performance. However, the feature values of a texture image vary with the scale, it is difficult to know if a query texture image has the same scale as the target images. Recently, Quan *et al.* [19] proposed a multi-scale LBP based global fractal feature to solve the scale issue. But this feature is not robust for small sized images. Li *et al.* [31] proposed a technique to find the optimal scale for each pixel and extracted LBP feature with the optimal scale. However, it failed to extract accurate and consistent scale for all pixels. To extract scale invariant feature Guo *et al.* [32] proposed scale selective complete local binary pattern (SSCLBP). Although their reported results are quite impressive, they did not establish the relation between image structure and scale parameter.

Noise, which introduces additional geometric variation, can also create problems for texture image recognition. Hence, noise tolerant and robust texture recognition problem drew attention of the research communities. Tan and Triggs [33] introduced local ternary pattern (LTP) which is more resistant to noise. But LTP is not strictly invariant to gray-scale changes. Ren *et al.* [34] proposed a more efficient noise resistant local binary pattern (NRLBP) scheme based on LBP, but it is computationally expensive to generalize to larger scales with more number of neighboring points. Liu *et al.* introduced binary rotation invariant and noise tolerant (BRINT) feature [35]. However to calculate BRINT, they used a multi-scale approach which is computationally expensive and suffers from high dimensionality problem. To the best of our knowledge, no work is reported in the literature that deals with invariance to scale, translation, rotation, or reflection and insensitive to noise of a texture image. To achieve such invariance properties, it is appeared that local patterns from a Jet Space [36] of the image may be useful. Based on this assumption, we propose here an effective local jet space descriptor, named as local jet pattern (LJP). To extract the LJP, at first the Jet Space of a texture image is derived by convolving the derivative of Gaussian (DtGs) kernels upto 2^{nd} order. Then, the LJP for each element of Jet Space is build by exploiting the local relationships in that space. Finally, for a texture image, the normalized feature vector is formed by concatenating histogram of LJP for all elements of the Jet Space. The main contributions of this paper can be summarized as follows,

- We propose a simple, effective, yet robust jet space based texture descriptor called local jet pattern (Sec. III) for texture classification. In jet space the properties of Hermite polynomial are utilized to make DtGs responses for preserving the intrinsic local image structure in hierarchical way.
- The LJP descriptor achieves sufficient invariance to ad-

dress the challenges of scale, translation, and rotation (or reflection) for texture classification. In addition, the proposed descriptor is also robust to the noise variations (Subsec. II-B).

- The proposed algorithm takes very reasonable amount of time in feature extraction stage.
- We experimented and observed that the proposed descriptor outperforms the traditional LBP and other state-of-the-art methods on different texture databases, such as KTH-TIPS and CURET (Sec. IV) etc.

The rest of the paper is organized as follows. Sec. II deals with the mathematical definition of a broad class of local image decompositions, jet and jet space norm. The proposed LJP feature extraction scheme is presented in Sec. III. In Sec. IV the performance of texture classification is compared with the state-of-the-art methods. Finally, concluding remarks are drawn in Sec. V.

II. IMAGE STRUCTURE ANALYSIS, JETS AND JET SPACE

In order to support recognition of several image structures embedded in image data and to serve as a precursor for more detailed analysis, such as defining a local orientation or scale, or labelling a region as “corner”, “edge” etc., a local image structure analysis is demanded. A general framework to deal with image structures at different resolution, the Scale Space representation is introduced in [37]–[39]. Mathematical ideas of “local deep structure” [40] are informally linked to the concept of derivative, formally defined as follows,

$$I'(0) = \lim_{\Delta \rightarrow 0} \frac{I(0 + \Delta) - I(0)}{\Delta}$$

and thus, it is inapplicable to discrete functions, such as images, that are the result of physical measurement. Scale space analysis [39] introduces a two-step solution for image derivative measurement as follows:

First, a way of changing the inner scale of an image is defined, by convolving (denoted by $*$) the image with Gaussian kernels. The 1D Gaussian kernels of scale $\sigma \in \mathbb{R}^+$ are defined as

$$G_{\sigma}(x) = \frac{1}{\sigma\sqrt{2\pi}} \exp \frac{-x^2}{2\sigma^2}$$

As the 2D Gaussian function is separable [41], [42], its convolution with the input image can be efficiently computed by applying two passes of the 1D Gaussian function in the horizontal and vertical directions:

$$G_{\sigma}(x, y) = G_{\sigma}(x)G_{\sigma}(y).$$

The scaling operation to obtain $I_{\sigma} = G_{\sigma} * I$ can be computed efficiently and stably because of the magnificent localization of the Gaussian both in space and frequency [43] even if the input image (I) is the result of physical measurement, so called directly sampled [40].

Secondly, the Scale Space approach to calculate image derivative of a rescaled image can be done alternatively by convolving the original image with a derivative of Gaussian (DtG) ($I'_{\sigma} = G'_{\sigma} * I$) as proposed by Young [44]. He showed that Gaussian derivatives fit more accurately for the measurement of image structure at the receptive fields than the other

function such as Gabor function does. The DtGs at scale $\sigma > 0$ are defined in 1D by

$$G_\sigma(x) = G_\sigma^0(x) = \frac{1}{\sigma\sqrt{2\pi}} \exp\left(-\frac{x^2}{2\sigma^2}\right)$$

$$G_\sigma^m(x) = \frac{d^m}{dx^m} G_\sigma(x)$$

$$= \left(\frac{-1}{\sigma\sqrt{2}}\right)^m \mathbf{H}^m\left(\frac{x}{\sigma\sqrt{2}}\right) G_\sigma(x), m \in \mathbb{Z}^+ \quad (1)$$

where $G_\sigma^0(x)$ is the original Gaussian, m is a positive integer, and $H^m(x)$ is the n^{th} order Hermite polynomial (Fig. 1(a)) [45]. It is also useful to perform normalizations of the DtGs, such that $\int |G_\sigma^k(x)| dx = 1$. In particular, $G_\sigma^0(x)$ and $G_\sigma^1(x)$ are the ℓ^1 -normalized blurring and differentiating filters, respectively. Hermite transform was originally developed for the mathematical modelling of the properties of early stages of (human) vision [45]. From the properties of the Hermite polynomials, one sees that the neighborhood functions for even order are *symmetrical* ($G_\sigma^m(-x) = G_\sigma^m(x)$), whereas these for odd order are *anti-symmetrical* ($G_\sigma^m(-x) = -G_\sigma^m(x)$). The evaluation of the results of the neighborhood operators (that is, the $G_\sigma^m(x)$) all over an image, it pays to move to the Fourier domain: The Fourier representation of a convolution with the n^{th} order operator becomes a multiplication with an n^{th} power times a Gaussian frequency envelope, which leads to practical implementations. The DtGs at scale $\sigma > 0$ are defined in 2D (Fig. 1(b)) by

$$G_\sigma^{(m,n)}(x,y) = G_\sigma^m(x) G_\sigma^n(y), \quad m, n \in \mathbb{Z}^+ \quad (2)$$

$$G_\sigma(x,y) = G_\sigma^{(0,0)}(x,y)$$

Thus the scale-space approach allows computation of image

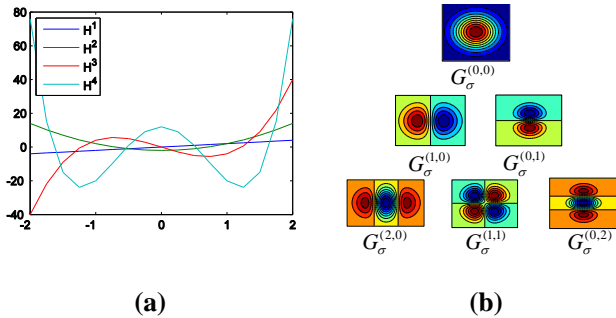


Figure 1: (a) Hermite polynomial of different orders. (b) The 2-D derivatives of the Gaussian (DtGs) upto 2^{nd} order.

derivatives of any order at any scale. The convolution formalism should be used when derivatives across the entire image are required, whereas an inner product formalism ($\langle \cdot | \cdot \rangle$) is more convenient if derivative at a single location is required. For instance, the image derivatives at scale σ , with respect to the origin is defined as follows,

$$J_{(m,n)} = (-1)^{(m+n)} \langle G_\sigma^{(m,n)} | I \rangle$$

$$= (-1)^{(m+n)} \int_{x,y \in \mathbb{R}} G_\sigma^{(m,n)}(x,y) I(x,y) dx dy. \quad (3)$$

Note that the image derivative measurements $J_{m,n}$ (Fig. 2) are dependent on the inner scale σ , though we do not indicate it

with a superscript to prevent cluttered equations. Furthermore, we get scale normalized DtGs response ($J_{(m,n)}^s$) by multiplying σ^{n+m} with the corresponding $J_{(m,n)}$ represented as,

$$J_{(m,n)}^s = \sigma^{n+m} J_{(m,n)}. \quad (4)$$

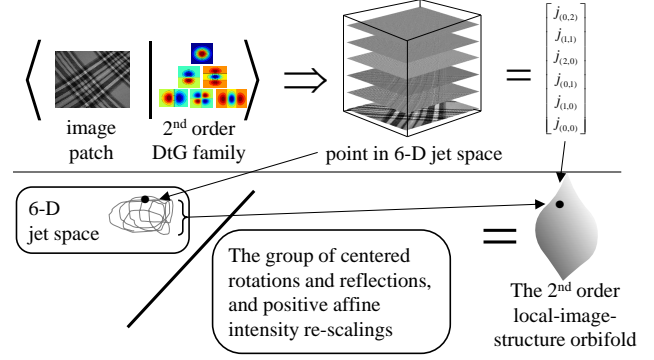


Figure 2: Diagrammatically, (top-left) the measurement of image structure using a bank of DtG filters up to second order and the resulting jet (top-right).

It is noted that the DtGs are not orthonormal kernel (e.g., $\langle G_\sigma^{(2,0)} | G_\sigma^{(0,2)} \rangle = 1/(16\pi\sigma^6)$) to avoid incorrect presumption. Typically, one measures with a family of DtG filters with some order. For the structure up to k^{th} order, $\{G_\sigma^{(m,n)} | 0 \leq m+n \leq k\}$, the vector of DtGs responses $J_{(m,n)}^k = \langle G_\sigma^{(m,n)} | I \rangle$ is referred to as a local \mathcal{L} -jet, where $J_{(m,n)}^k \in \mathbb{R}^{\mathcal{L}}$, $\mathcal{L} = \frac{(k+2)!}{2 \cdot k!}$ and is said to be an element of jet space [36]. Here we are only concerned up to 2^{nd} order structure, the measurements of which requires a set of six DtG kernels denoted as, $\{\vec{G} = (G_\sigma^{(0,0)}, G_\sigma^{(1,0)}, G_\sigma^{(0,1)}, G_\sigma^{(2,0)}, G_\sigma^{(1,1)}, G_\sigma^{(0,2)})\}$, henceforth, called the DtG family (shown in Fig. 1(b)). The DtG responses calculated from Eqn. (4) are denoted as $\{\vec{J} = (J_{(0,0)}^s, J_{(1,0)}^s, J_{(0,1)}^s, J_{(2,0)}^s, J_{(1,1)}^s, J_{(0,2)}^s)\}$ is called a 6-jet (shown in Fig. 2 (top-left)). We denote $\vec{J} = \langle \vec{G} | I \rangle$ for the jet arising from the image response I . Fig. 3 shows an example of image patches whose local structure is dominated by higher orders (up to 2^{nd} order).

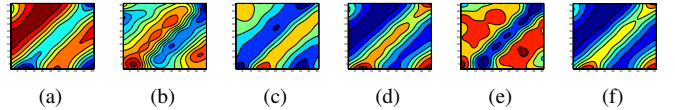


Figure 3: (a)-(e). Example of different type of local structure upto 2^{nd} order for image patch as shown Fig. 2

A. Effects of Similarity Transforms

In computer vision problems, a group of transforms are typically chosen to analyse the effect of geometrical structure those are invariant with respect to scaling, translation, rotation and reflection of an image, a constant intensity addition, and multiplication of image intensity by a positive factor and their combinations. In order to cope with the translation effect, we choose the analyzing point as the origin of the co-ordinate system.

In the jet space, Gaussian derivatives are represented by Hermite polynomials multiplied with Gaussian window (in Eqn. (1)). The details within the window is expanded over the basis of Hermite polynomials, therefore even if the scale (σ) is fixed, it provides a multi-scale hierarchical image structure for \mathcal{L} -jet [46]

Rotation of a surface is a more difficult problem in image analysis. Consider the rotation effect on jet about the origin with an angle θ . Here the zero order derivative term of the jet ($J_{(0,0)}$) remains unaffected. The first order derivative terms are transformed as follows,

$$\begin{pmatrix} J_{(1,0)} \\ J_{(0,1)} \end{pmatrix} \rightarrow \begin{pmatrix} \cos \theta & \sin \theta \\ -\sin \theta & \cos \theta \end{pmatrix} \begin{pmatrix} J_{(0,1)} \\ J_{(1,0)} \end{pmatrix}$$

and the second order terms are transformed according to

$$\begin{pmatrix} J_{(2,0)} \\ J_{(1,1)} \\ J_{(0,2)} \end{pmatrix} \rightarrow \frac{1}{2} \begin{pmatrix} 1+b & 2c & 1-b \\ -c & 2b & c \\ 1-b & -2c & 1+b \end{pmatrix} \begin{pmatrix} J_{(0,2)} \\ J_{(1,1)} \\ J_{(2,0)} \end{pmatrix}$$

where $b = \cos 2\theta$ and $c = \sin 2\theta$. So, to return the starting values, the first order derivative structure requires a full 2π rotation, while the second order derivative structure returns after a rotation by π .

In case of reflection (i.e. the effect of jet about the line $y = x$), the zero order term of the jet is not affected. However, the first order derivative term is transformed according to, $J_{(1,0)} \longleftrightarrow J_{(0,1)}$ and the second order derivative term, according to $J_{(2,0)} \longleftrightarrow J_{(0,2)}$. Considering all the DtGs responses together, the \mathcal{L} -jet ($\mathcal{L} = 6$) achieves invariance to scale, rotation, or reflection.

Image structure analysis may be appropriate if it considers that intensities are non-negative unconstrained real numbers, and also do not exceed a maximum value. Therefore, the image structure should not be affected by adding a constant (α) to all intensities as in case of uniform illumination change. When such changes arise, only the zero order derivative term is affected and it simply transforms according to, $J_{(0,0)} \rightarrow J_{(0,0)} + \alpha$.

It is also required that the image local structure should be invariant to the multiplication by a non-zero positive factor ($\epsilon > 0$) with all image intensities. In this case, the factor is simply multiplied with all terms of jet vector i.e., $\vec{J} \rightarrow \epsilon \vec{J}$. Note that, it does not require multiplication of intensities by a negative factor to make it invariant to physical constraints.

B. Jet Space Norm

A jet space norm ($\|\cdot\|$) is a function which associates each element with a positive number and expresses the image structure magnitude measured by the jet [47]. The Jet space norm plays an important role in texture analysis. This norm is developed by characterizing the requirements as follows,

- The norm should satisfy the standard axioms for a semi-norm (\mathbf{R}_1).
- The norm should be invariant under translation, rotation, and reflection of the image domain (\mathbf{R}_2).
- The norm should not be affected by uniform illumination changes in the image (\mathbf{R}_3).

First, consider some standard norms rather than jets, which help us to define the jet space norm. The ℓ_2 -norm (satisfying \mathbf{R}_3), is the most commonly used norm and written as,

$$\|I\|_2 = (\langle 1|I^2 \rangle - \langle 1|I \rangle^2)^{\frac{1}{2}}$$

The common variation for function norms, is not to evaluate the function over the entire domain, rather, only over some subregion of the domain. Generally, a weighted function (ω) is used to provide importance of different parts of the domain that are relevant to the norm, i.e.

$$\|I\|_{\omega} = (\langle \omega|I^2 \rangle - \langle \omega|I \rangle^2)^{\frac{1}{2}}$$

In scale space framework, this norm is a common choice when the weighted function is a Gaussian [48]. The scale space norm of an texture image (I) with a Gaussian weighted function, evaluated at the origin, with scale $\sigma > 0$, can be define as

$$\|I\|_{\sigma} = (\langle G_{\sigma}|I^2 \rangle - \langle G_{\sigma}|I \rangle^2)^{\frac{1}{2}}$$

Since the jet does not specify an image that can be windowed, therefore scale-space norm cannot be applied directly to the jets [49]. In fact, jets specify the metamery class of all the images. There is no upper bound on the scale space norm of the members of a metamery class, however there is a unique norm minimizer. The jet space norm is defined as minimum of the Scale Space norms for the elements of the metamery class defined by jet. The jet space norm can be derived on the form of norm minimizer [47] as follows, "Of all the functions that measure to a particular jet \vec{J} of order k , that uniquely minimizes the scale space norm is"

$$Q_{\vec{J}} = J_{(0,0)} + \sum_{1 \leq m+n \leq k} J_{(m,n)} \frac{(2^{-\frac{1}{2\sigma}})^{(m+n)}}{m!n!} \mathbf{H}^m\left(\frac{x}{\sigma\sqrt{2}}\right) \mathbf{H}^n\left(\frac{y}{\sigma\sqrt{2}}\right).$$

and the norm of the second order jet is written as,

$$\|\vec{J}\| = \left(\sigma^2 (J_{(1,0)}^2 + J_{(0,1)}^2) + \frac{1}{2} \sigma^4 (J_{(2,0)}^2 + 2J_{(1,1)}^2 + J_{(0,2)}^2) \right)^{\frac{1}{2}}.$$

This norm satisfies the requirements of $\mathbf{R}_1 - \mathbf{R}_3$ and the magnitude of the local structure measured by the jet as desired.

III. PROPOSED DESCRIPTOR

Although the original LBP scheme is attractive for its conceptual simplicity and efficient computation, an effortless application of the original $\text{LBP}_{R,N}$ histogram descriptor has the following limitations,

- 1) The original $\text{LBP}_{R,N}$ operator produces rather long histogram, 2^N different values, overwhelmingly large even for small neighborhoods, as shown in Table I leading to poor discriminant power and larger storage requirements.
- 2) The original $\text{LBP}_{R,N}$ codes are often sensitive to image rotation.
- 3) $\text{LBP}_{R,N}$ codes can be highly sensitive to noise: the slightest fluctuation above or below the value of the central pixel is treated similar to a major contrast.

Even the sampling method is similar to that in LBP, we propose a simple, efficient, yet robust descriptor, called local jet pattern (LJP) for texture recognition to overcome the

Table I: Number of Patterns of Different Descriptors

Scale	(R , N)	$\text{LBP}_{R,N}$	$\text{LBP}_{R,N}^{r1}$	$\text{LBP}_{R,N}^{u2}$	$\text{LBP}_{R,N}^{riu2}$	CLBP_CSM
1	(1, 8)	256	36	59	10	200
2	(2, 16)	65536	4116	243	18	648
3	(3, 24)	16777216	699252	—	26	1352
4	(4, 32)	2^{32}	large	—	34	2312
5	(5, 40)	2^{40}	large	—	42	3528
1-5		infeasible	infeasible		106	8040

forementioned problem and to address together 1) invariance to scale, translation, and rotation (or reflection), 2) noise tolerance of a texture image. The proposed method is explained as follows.

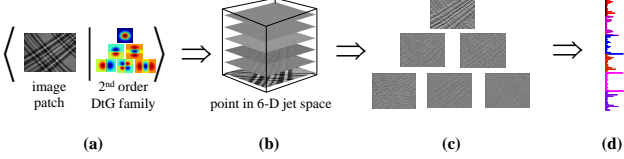


Figure 4: (b) The response of DtGs (i.e., local jets vector (LJV)) upto 2^{nd} order of a texture image. (c) The local jet pattern ($\text{LJP}_{R,N}^{i,j,l} | l = 1, 2, \dots, \mathcal{L}$) for individual element of Local Jet Vector (LJV). (d) Final LJP feature vector obtained by concatenating all $H_{R,N}^l$ where $l = 1, 2, \dots, \mathcal{L}$.

A. Local Jet Pattern

There is no particular spatial scale at which a natural image should be preferably analyzed. The potential feature points are detected by searching over all scales and image locations. Detecting locations that are invariant to the scale change of the image can be accomplished by searching for stable features across all possible scales, using a continuous function of scale, known as scale space. It is therefore desirable to represent the image in a scale space, so that a range of resolutions can be considered. The preferred way to do this is by constructing the local jet pattern (LJP), it follows that the structure of the image, at a given scale, can be analyzed by the spatial derivatives of the corresponding texture image with different isotropic and anisotropic Gaussian structure. We use here multi-scale \mathcal{L} -jet as described by Florack *et al.* [36]. The multi-scale local jet representation of an image is formed not only using the spatial derivatives, but also including derivatives with respect to the scale (σ). A jet space representation of a texture image is derived from a set of derivative of Gaussian (DtGs) filter responses up to second order, so called local jet vector (LJV), which also satisfies the properties of Scale Space. In other words, the jet can also be interpreted as isolating an image patch with a Gaussian window and then probing it with Hermite function - which is not unlike a windowed Fourier transform. To obtain LJP, initially, we transform the candidate texture image into local \mathcal{L} -jet ($\mathcal{L} = 6$) using Eqn. (2), where the element of jet represents the responses of the DtGs (discussed in Section-II) upto 2^{nd} order. The scale normalized derivative of 6-jet for a given image I are $\{\vec{J} = (J_{(0,0)}^s, J_{(1,0)}^s, J_{(0,1)}^s, J_{(2,0)}^s, J_{(1,1)}^s, J_{(0,2)}^s)\}$ represented as a vector $\{\vec{J} = (J^1, J^2, \dots, J^{\mathcal{L}-1}, J^{\mathcal{L}})\}$ which we refer as the local jet vector (LJV). The local jet pattern (LJP) are computed after a contrast normalization preprocessing step, motivated by Weber's law [7]. Let $\|J^{(i,j)}\|$ be the ℓ_2 norm

of the DtGs responses at pixel (i, j) . We normalize the DtGs responses as follows,

$$\mathbf{J}^{(i,j)} \leftarrow \mathbf{J}^{(i,j)} \times \frac{\log(1 + \frac{L^{(i,j)}}{0.03})}{L^{(i,j)}}, \quad (5)$$

where $L^{(i,j)} = \|\mathbf{J}^{(i,j)}\|_2$ is the magnitude of the DtGs response at that pixel.

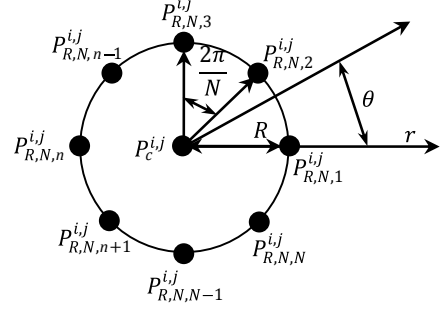


Figure 5: The local neighbors $P_{R,N,n}^{i,j}$ for $(\forall n \in [1, N])$ of a center pixel $P_c^{i,j}$ in polar coordinate system.

Finally, the local jet pattern (LJP) for each element in the jet vector for a given center pixel $P_c^{i,j}$ at (i, j) is computed by comparing its gray value $J_c^{i,j}$ with the gray value of a set of N local circularly and equally spaced neighbors $P_{R,N}^{i,j}$ with radius R around the center pixel $P_c^{i,j}$ (Fig. 5). LJP considers only those pixel as a center pixel whose all N local neighbors are within the image in jet space of dimension $M_x \times M_y$. In Fig. 5, the n^{th} neighbor of $P_c^{i,j}$ (i.e. n^{th} element of $P_{R,N}^{i,j}$) is denoted by $P_{R,N,n}^{i,j}$ having gray value $J_{R,N,n}^{i,j}$, where n is a positive integer and $n \in [1, N]$. The spatial coordinate (x, y) of $P_{R,N,n}^{i,j}$ with respect to the origin of the image is given as,

$$\begin{aligned} x(P_{R,N,n}^{i,j}) &= i + r(P_{R,N,n}^{i,j}) \times \cos(\theta(P_{R,N,n}^{i,j})) \\ y(P_{R,N,n}^{i,j}) &= j - r(P_{R,N,n}^{i,j}) \times \sin(\theta(P_{R,N,n}^{i,j})) \end{aligned} \quad (6)$$

where $i \in [R+1, M_x - R]$ and $j \in [R+1, M_y - R]$. $r(P_{R,N,n}^{i,j})$ and $\theta(P_{R,N,n}^{i,j})$ denote the polar coordinates of $P_{R,N,n}^{i,j}$ where $n = 1, 2, \dots, N$ and are computed as

$$\begin{aligned} r(P_{R,N,n}^{i,j}) &= R \\ \theta(P_{R,N,n}^{i,j}) &= (n-1) \times \frac{2\pi}{N} \end{aligned} \quad (7)$$

Let $J_c^{i,j,l}$ be a center pixel (i, j) of l^{th} element of jet vector ($l \in [1, \mathcal{L}]$) and $J_{R,N,n}^{i,j,l}$ is the n^{th} neighbor of $J_c^{i,j,l}$ corresponding to the N sampling points with radius R and the array of N neighbors defined as,

$$\vec{J}_{R,N}^{i,j,l} = [J_{R,N,1}^{i,j,l}, J_{R,N,2}^{i,j,l}, \dots, J_{R,N,N}^{i,j,l}]$$

The LJP response for a given center pixel $J_c^{i,j,l}$ of l^{th} element of local jet vector (LJV) is calculated as,

$$\text{LJP}_{R,N}^{i,j,l} = \sum_{n=1}^N 2^{n-1} \times \text{sign}(J_{R,N,n}^{i,j,l} - J_c^{i,j,l}) \quad (8)$$

where sign is a *unit step* function to denote whether a given input is positive or not, and is defined as,

$$\text{sign}(z) = \begin{cases} 1, & z \geq 0 \\ 0, & z < 0 \end{cases}$$

Note that the range of LJP depends on the number of neighboring sampling point (N) around its center $J_{R,N}^{i,j,l}$ at radius R to form the pattern and its value lies in between 0 to 2^{N-1} . In other words, the range of LJP is $[0, 2^{N-1}]$. We compute the LJP for all elements of LJV. Fig. 4(c) shows the computed local jet patterns (i.e. $\text{LJP}_{R,N}^{i,j,l} | l = 1, 2, \dots, \mathcal{L}$) from each element of LJV (Fig. 4(b)) for a candidate texture image (Fig. 4(a)).

B. LJP Feature Vector

To reduce the computation classification cost using local jet pattern (LJP) of a texture image, we need to compute the frequency of local jet pattern (LJP) for each element of local jet vector (LJV) ($\bar{J} = (J^1, J^2, \dots, J^{\mathcal{L}-1}, J^{\mathcal{L}})$). The frequency of local jet pattern (LJP) (H) of 2^N dimension is calculated for every pixel of LJP image I of size $(M_x \times M_y)$. The normalized LJP histogram feature vector ($H_{R,N}^l$) for $l^{th} \in [1, \mathcal{L}]$ element of LJV when N neighbors at radius R are considered to construct the $\text{LJP}_{R,N}^{i,j,l}$ are computed using the following equation,

$$H_{R,N}^l(\Omega) = \sum_{i=R+1}^{M_x-R} \sum_{j=R+1}^{M_y-R} f(\text{LJP}_{R,N}^{i,j,l}(i, j), \Omega) \quad (9)$$

where $\forall \Omega \in [0, 2^N - 1]$ and $f(u, v)$ is a function given by

$$f(u, v) = \begin{cases} 1, & \text{if } u == v \\ 0, & \text{otherwise.} \end{cases}$$

The final LJP feature vector is constructed by concatenating all $H_{R,N}^l$ where $l = 1, 2, \dots, \mathcal{L}$. Since the number of bins in Eqn. (9) of $\text{LJP}_{R,N}^{i,j,l}$ for each element of LJV ($l \in [1, \mathcal{L}]$) is 256 when $R = 1, N = 8$, the length of the LJP feature vector dimension becomes as high as, $256 \times 6 = 1536$. In order to reduce the number of bins we adopted *uniform* pattern scheme [22], which gives 59 bins for each element of LJV and the dimension of final normalized LJP feature vector is reduced to $59 \times 6 = 354$. Since the zeroth order term of DtGs response does not carry any geometrical information, it is discarded. Therefore, the feature vector dimension is further reduced to $59 \times 5 = 295$.

From Subsec. II-A, we observed that $J_{(0,0)}$ and $J_{(1,1)}$ of LJV are invariant to rotation, or reflection individually. Now, considering LJP for all the elements of LJV, i.e. \mathcal{L} -jet ($\mathcal{L} = 6$) together, is invariant to scale, rotation, or reflection of the image surface. Therefore, the final LJP feature vector is also invariant to scale, rotation, or reflection of the texture image.

We computed and compared the probability distributions of feature vectors difference of proposed and state-of-the-art features using sample images of intra and inter class and shown in Fig. 6. The horizontal axis indicates the deviation from zero mean and the vertical axis indicates the probability of feature vector difference for one sample image to another by a particular amount of deviations. The probability at zero

mean with high amplitude represents higher similarity between feature vectors whereas larger deviation from zero mean implies the less similarity. Fig. 6 shows that LJP is more discriminative as it perfectly differentiates inter class variations (Sample1 and Sample3) and at the same time better matches for intra class images (Sample1 and Sample2).

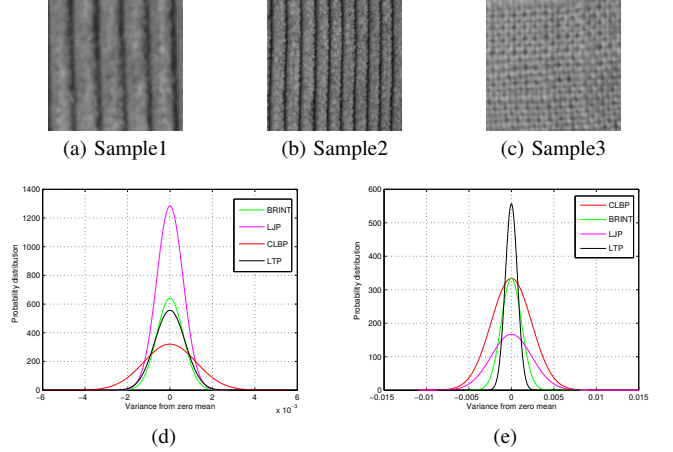


Figure 6: Illustration of the behavior of LTP, BRINT, CLBP, and LJP for inter and intra class sample images; (a)-(c) Three texture images taken from KTH-TIPS [50] texture database where Sample1 and Sample2 belong to the same class whereas Sample1 and Sample3 belong to the different classes; (d)-(e) represents the probability distributions of feature vectors difference with respect to zero mean of different methods for intra and inter class images respectively.

Assuming image of size $M_x \times M_y$ and the kernel of size $P \times Q$, the algorithmic complexity of the proposed descriptors computed as follows. To create the \mathcal{L} -jet representation of input image in step 4 of Algorithm 1 requires roughly $\mathcal{L}M_xM_yPQ$ multiplications and additions. As 2-D DtGs kernel is separable, filtering is done in two steps. The first step requires about $\mathcal{L}M_xM_yP$ multiplications and additions while the second requires about $\mathcal{L}M_xM_yQ$ multiplications and additions, making a total of $\mathcal{L}M_xM_y(P+Q)$. Since \mathcal{L} and kernel size is constant, the complexity becomes $O(M_xM_y)$. The creation of LJP pattern, as presented in step 11 of Algorithm 1, requires roughly $\mathcal{L}NM_xM_y$ multiplications and additions, and complexity becomes $O(M_xM_y)$, where N is the number of even space circular neighbor pixels to each center. As step 13 of Algorithm 1 takes $O(M_xM_y)$ to create histogram of LJP, the time complexity of proposed LJP descriptor is $3M_xM_y \approx O(M_xM_y)$.

C. Comparing Distribution of local Descriptor

After computing the LJP descriptors as elaborated in the previous section, we need to represent their distributions in the training (model) and test (sample) images. The dissimilarity of sample and model histograms is a test of goodness-of-fit, which can be measured with a non-parametric statistical test. There are many metrics for evaluating the fit between two histograms, such as histogram intersection, log-likelihood ratio, and chi-square (χ^2) statistic [22]. In this paper, the actual classification is performed via two non-parametric classifiers. First, the nearest neighbor classifier (NNC) with

Algorithm 1: Algorithm to extract $LJP_{R,N}^{i,j,l}$ descriptor, where N is the number of circular sample at radius R .

Data: The texture image (I)

Result: Normalized Local Jet Pattern (HLJP) Descriptor

```

1 initialization ( $R = 1, N = 8, k = 2, m = 0, n = 0$ );
2 while ( $m \leq 2$  and  $n \leq 2$  and  $(m + n) \leq 2$ ) do
3   Create DtGs Kernel ( $G_{\sigma}^{m,n}$ ) upto  $k = 2^{nd}$  Order;
4    $J_{(m,n)} = (-1)^{m+n} \langle G_{\sigma}^{m,n} | I \rangle$ ;
5 end while
6  $J_{(m,n)}^s = \sigma^{m+n} J_{(m,n)}$ 
7 initialization ( $i = R+1, j = R+1, l = 1, \mathcal{L} = \frac{(k+2)!}{2 \times k!}$ );
8 while ( $l \leq \mathcal{L}$ ) do
9   while ( $i \leq M_x - R$  and  $j \leq M_y - R$ ) do
10     $\mathbf{J}^{(i,j,l)} \leftarrow \mathbf{J}^{(i,j,l)} \times \frac{\log(1 + \frac{L^{(i,j)}}{0.03})}{L^{(i,j)}}$ ;
11     $LJP_{R,N}^{(i,j,l)} = \sum_{n=1}^N 2^{(n-1)} \times \text{sign}(J_{R,N,n}^{i,j,l} - J_c^{i,j,l})$ ;
12  end while
13   $H_{R,N}^l = \text{HIST}(LJP_{R,N}^{i,j,l})$ ;
14   $HLJP = \text{concatenateNormalizeLJP}(H_{R,N}^l)$ ;
15 end while

```

the chi-square (χ^2) distance [4], [7], [27] is used to show the effectiveness of the proposed feature extraction scheme. To compare two histograms $H_1 = u_1, \dots, u_M$ and $H_2 = w_1, \dots, w_M$, we use the χ^2 distance defined as,

$$D(H_1, H_2) = \sum_{i=1}^M \frac{(u_i - w_i)^2}{u_i + w_i} \quad (10)$$

where M is the number of bins, H_1 and H_2 are the extracted features of a test sample and a model, respectively. The class of test sample H_1 is assigned to the class of model H_2 that minimizes the χ^2 -distance.

Then another advanced classifier, called nearest subspace classifier NSC [51], is implemented to further improve the classification performance. In order to avoid the over emphasizing patterns with large frequency, a preprocessing step is applied to the proposed feature before NSC, similar to that in [32]:

$$\bar{X}_m = \sqrt{X_m}, \quad m = 1, 2, \dots, M \quad (11)$$

where M is the number of bins, and X_m is the original frequency of the LJP at m^{th} bin. The nearest subspace classifier (NSC) first calculates the distance from the test sample y to the i^{th} class and measures the projection residual r_i from y to the orthogonal principle subspace $B_i \in \mathbb{R}^{M \times m}$ of the training sets X_i , which is spanned by the principal eigenvectors of $\sum_i = X_i X_i^T$ for the i^{th} class, given as follows,

$$r_i = \|(I - P_{B_i})y\|_2 = \|(I - B_i B_i^T)y\|_2 \quad (12)$$

where $P = I \in \mathbb{R}^{M \times M}$ is a identity matrix where M rows are selected uniformly at random. The test sample y is then assigned to the one of the C classes with the smallest residual among all classes, i.e.

$$i^* = \arg \min_{i=1, \dots, C} r_i \quad (13)$$

IV. EXPERIMENTAL EVALUATION

A. Texture Databases

To evaluate the effectiveness of the proposed descriptor, we carried out a series of experiments on five large and commonly used texture databases: Outex_TC-00010 (TC10) [52], Outex_TC-00012 (TC12) [52], Brodatz album [53], KTH-TIPS [50], and CURET [54] texture databases. The Brodatz database is perhaps the best known benchmark for evaluating texture classification algorithms. Performing classification on entire databases is challenging due to relatively large number of texture classes, the small number of examples for each class, and the lack of intra-class variation.

The performance of different methods are evaluated in term of classification accuracy using K-fold cross-validation test along with two non-parametric classifier, nearest neighbor classifier (NNC) with Chi-Square (χ^2) distance and nearest subspace classifier (NSC). In K-fold cross-validation, the feature set is randomly sorted and divided into K-folds ($K = 10$). The average of the classification accuracies over K rounds get a final cross-validation accuracy. The K-fold cross-validation process provides a more accurate picture of the classification performance. The performance of the proposed descriptor is compared with $LBP_{R,N}$ [22], $LBP_{R,N}^{u2}$, $DLBP_{R,N}$ [26], $LBP_{R,N}^{sri-su2}$ [31], multiscale $CLBP_{R,N}^{riu2}/M_{R,N}^{riu2}/C(1, 8 + 3, 16 + 5, 24)$ [27] and STATE-OF-THE-ART methods. Each image sample is preprocessed: normalized to have an average intensity of 128 and a standard deviation of 20 [22], whereas in VZ-MR8 and VZ-Patch methods, the texture samples are normalized to have an average intensity of 0 and a standard deviation of 1 [6], [7], [14]. This is done to remove the global intensity and contrast.

Table II: Summary of Texture Database used in Experiment #1

Texture Database	Image Rotation	Illumination Variation	Scale Variation	Texture Classes	Sample Size (pixels)	Samples per Class	Total Samples
Outex_TC10	✓			24	128 x 128	180	4320
Outex_TC12	✓	✓		24	128 x 128	200	4800

EXPERIMENT #1: There are 24 different homogeneous texture classes selected from the Outex texture databases [52], each having the size of 128×128 pixels. **Outex_TC_00010 (Outex_TC10)** contains texture images under illuminant “inca” whereas **Outex_TC_00012 (Outex_TC12)** contains texture images with 3 different illuminants (“inca”, “horizon”, and “t184”). Both of the Outex test suits images are collected under 9 different rotation angels ($0^\circ, 5^\circ, 10^\circ, 15^\circ, 30^\circ, 45^\circ, 60^\circ, 75^\circ$, and 90°) in each texture class. The test suites **Outex_TC_00010 (Outex_TC10)**, and **Outex_TC_00012 (Outex_TC12)** are summarized in Table II.

EXPERIMENT #2: Brodatz [53] album is chosen to allow a direct comparison with the state-of-the-art results [26]. There are 32 homogeneous texture classes*. Each image is partitioned into 25 non-overlapping sub-images of size 128×128 , each of these is down-sampled to 64×64 pixels.

*The 32 Brodatz textures are Bark, Beachsand, Beans, Burlap, D10, D11, D4, D51, D52, D5, D6, D95, Fieldstone, Grass, Ice, Image09, Image15, Image17, Image19, Paper, Peb54, Pigskin, Pressedcl, Raffia2, Raffia, Reptile, Ricepaper, Seafan, Straw2, Tree, Water, Woodgrain;

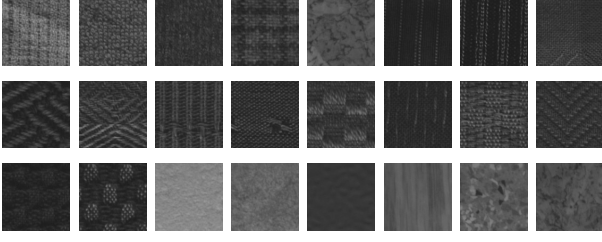


Figure 7: 24 texture images randomly taken from each class of Outex_TC10 and Outex_TC12 database

Table III: Summary of Texture Database used in Experiment #2

Texture Database	Image Rotation	Illumination Variation	Scale Variation	Texture Classes	Sample Size (pixels)	Samples per Class	Total Samples
KTH-TIPS	✓	✓	✓	10	200 x 200	81	810
Brodatz	✓		✓	32	64 x 64	64	2048
CUReT	✓	✓		61	200 x 200	92	5612

For **CUReT** [54] database, we used the same subset of images which contain 61 texture classes with 92 images per class [15], [4], [6]. It is designed to contain large intraclass variation and is widely used to assess the classification performance. The images are captured under different illumination and viewing directions with constant scale. All 92 images of 61 texture classes are cropped into 200×200 region and converted to gray scale [6].

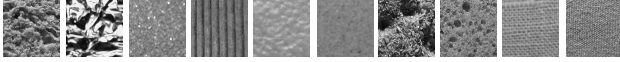


Figure 8: Ten texture images randomly taken from each class of KTH-TIPS database.

KTH-TIPS [50] database is extended by imaging new samples of ten of CUReT textures as shown in Fig. 8. It contains texture images with 3 viewing angles, 4 illuminations, and 9 different scales of size 200×200 . The **Brodatz**, **CUReT**, and **KTH-TIPS** databases are summarized in Table III.

B. Results of Experiment #1

The results of Experiment #1, carried out on Outex_TC10 and Outex_TC12 are tabulated in Table IV. This Table includes average classification accuracy of K -fold cross-validation test ($K = 10$) for the proposed descriptor and the comparative summary of the results for LBP_(R,N) [22], VZ-MR8 [6], VZ-Patch [7] and recent state-of-the-art methods. We have made the following observations from the results of Experiment #1. Though LBPV has the same feature dimension as LBP, the use of LBPV incorporates additional contrast measures to the pattern histogram and produces a significant performance compared to the original LBP. LBP_{R,N}^{riu2}/VAR_{R,N} provides better performance compared to LBPV_{R,N}^{riu2}. This is because LBP and local variance of a texture image are complementary and so, the strength is obtained with the joint distribution of LBP and local variance compared to one alone. CLBP_S^{riu2}/M_{R,N}^{riu2}/C(1,8 + 2,16 + 3, 24) which is made by fusing the CLBP_S and CLBP_{M/C}, provides better performance compared to other variant of CLBP. This is because it contains complementary features of sign and magnitude, in addition to center pixel which represents the

gray level of the local patch. DLBP + NGF, which make

Table IV: Average classification accuracy (%) on Outex_TC10 and Outex_TC12 using STATE-OF-THE-ART schemes

Method	Classifier	Outex_TC10	Outex_TC12 horizon	t184	Average
LTP [33]	NNC	76.06	63.42	62.56	67.34
VAR [21]	NNC	90.00	64.35	62.93	72.42
LBP [22]	SVM	97.60	85.30	91.30	91.40
LBP _{R,N} ^{riu2}	NNC	84.89	63.75	65.30	71.31
LBP/VAR	NNC	96.56	78.08	79.31	84.65
LBPV _{R,N} ^{riu2} [25]	NNC	91.56	77.01	76.62	81.73
CLBP _S	NNC	84.81	63.68	65.46	71.31
CLBP _M	NNC	81.74	62.77	59.30	67.93
CLBP _{M/C}	NNC	90.36	76.66	72.38	79.80
CLBP _S /M/C [27]	NNC	94.53	82.52	81.87	86.30
CLBP _S /M	NNC	94.66	83.14	82.75	86.85
CLBP _S /M/C	NNC	98.93	92.29	90.30	93.84
LBP _{R,N} ^{NT} [55]	NNC	99.24	96.18	94.28	96.56
DLBP _{R=3,N=24} [26]	SVM	98.10	87.40	91.60	92.36
BRINT _{Cs_Cm} [35]	NNC	99.35	97.69	98.56	98.12
VZ-MR8 [6]	Nsc	93.59	92.82	92.55	92.99
VZ-Patch [7]	Nsc	92.00	92.06	91.41	91.82
PTP [56]	NNC	99.56	98.08	97.94	98.52
Proposed LJP	NNC	99.95	99.97	99.81	99.91
Proposed LJP	Nsc	100	99.97	99.88	99.98

use of the most frequently occurred 80% patterns of LBP to improve the recognition performance compared to the original LBP_{R,N}^{riu2} but like VAR_{R,N} neglects the local spatial structure which is important for texture discrimination. It is worth mentioning that DLBP approach needs pre training stage and the dimensionality of the DLBP varies with the training samples. For comparison, we provide the best results of DLBP with $R = 3$ and $N = 24$ in Table. IV. The state-of-the-art statistical algorithm, VZ-MR8 and VZ-Patch takes dense response from multiple filters. However, the performance is quite low compared to the proposed LJP. In addition, the complexity of feature extraction and matching is quite high [7] compared to the proposed LJP because the MR8 needs to find 8 maximum responses after 38 filters convolving with the image and compares every 8-dimension vector in an image with all the textons to build histograms using clustering technique. The LBP_{R,N}^{NT} [55] based methods and BRINT [35] give better performance compared to other state-of-the-art LBP methods. However, the accuracies are lower than those obtained by our proposed LJP. This is mainly because LBP_{R,N}^{NT} extracts features by using locally rotation invariant LBP_{R,N}^{riu2} approach which produces only 10 bins and such small size of features can not represent each class well, while BRINT extracted large number of features from multiple resolution ($R = 1, 2, 3, 4$) by utilizing rotation invariant LBP_{R,N}^{riu2} approach, whereas it loses the global image information.

Finally, even the Outex test suits (Outex_TC10, Outex_TC12 (“horizon” and “t184”)) contain both illuminant and rotation variant of textures the proposed descriptor achieves performance in term of mean accuracy and standard deviations $100 \pm 0.0000\%$, $99.97 \pm 0.0732\%$ and $99.88 \pm 0.1314\%$ on three different suits, respectively. Note that the textures under different illuminant and different viewpoint usually have different micro structures. The comparative results in Table IV shows that the proposed descriptor provides better classification performance compared to other state-of-the-art methods. The better performance is due to the following attributes. To extract LJP, initially, a jet space representation of a texture image is derived from a set of derivative of Gaussian

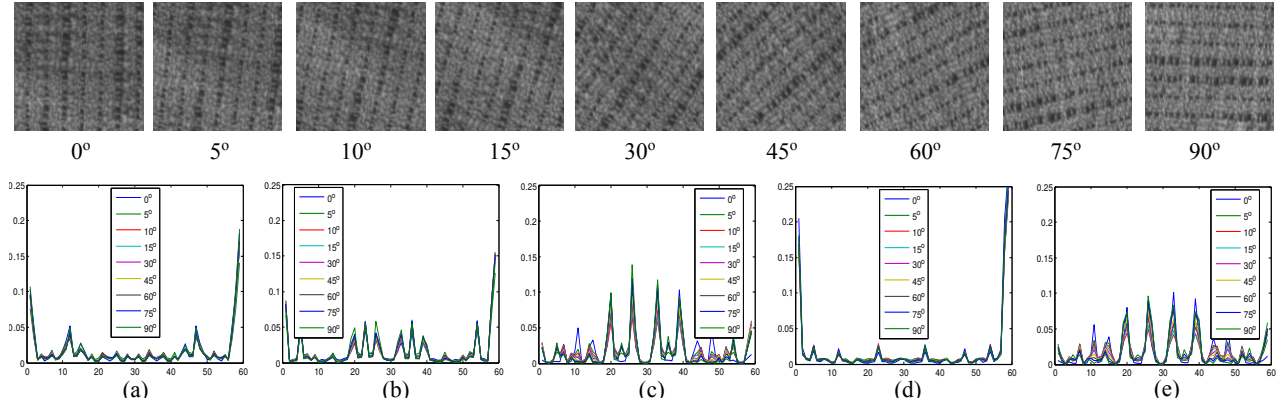


Figure 9: (a)-(e) represent individual LJP histograms ($H^l_{R,N} | l \in [2, \mathcal{L}]$) of a texture samples are taken from Outex database with 9 different orientations where abscissa and ordinate represent number of bins and feature probability distribution, respectively.

(DtGs) filter responses up to second order, so called local jet vector (LJV) (Fig. 4). Each element of LJV is encoded via *uniform* pattern scheme which produces 59 bins, are sufficient to discriminate each texture class. All the DtGs responses, LJV together achieve invariance to scale, rotation, or reflection and are able to capture the *micro structure* under different illumination controlled environment (“inca”, “horizon” and “t184”). To visualize the rotation invariant characteristic of the proposed descriptor, an example of LJP feature distribution for a texture samples taken from Outex_TC10 database having 9 different orientations ($0^\circ, 5^\circ, 10^\circ, 15^\circ, 30^\circ, 45^\circ, 60^\circ, 75^\circ$, and 90°) are shown in Fig. 9. Fig 9(a)-(e) represent the histograms ($H^l_{R,N} | l \in [2, \mathcal{L}]$) of individual ($LJP^{i,j,l}_{R,N} | l \in [2, \mathcal{L}]$). It is clearly observed that the LJP feature distribution of different orientations are approximately overlapped which signify the rotation invariance of LJP descriptor.

C. Results of Experiment #2

To analyse the scale invariance property of the proposed approach, we used the KTH-TIPS database which contains images with different scales. Each image of KTH-TIPS is captured in a controlled distance environment [50]. Fig. 10 shows an example texture image having 9 different scales to illustrate the effectiveness of scale invariance properties of LJP descriptor. Fig. 10(S¹)-(S⁹) show nine images of “corduroy” class in KTH-TIPS with different scales. Fig. 10(a)-(e) depict the histograms ($H^l_{R,N} | l \in [2, \mathcal{L}]$) of individual $LJP^{i,j,l}_{R,N}$ descriptor with $R = 1$, and $N = 8$. It is clear from Fig. 10(a)-(e) that the histograms of individual LJP for 9 different scales are approximately closed which imply that the LJP descriptor is scale invariant. The proposed descriptor achieves scale invariance by utilizing the properties of Hermite polynomials. As per Eqn. (1) the details within the Gaussian window is expanded over the basis of Hermite polynomials and this property provides a multi-scale hierarchical image structure for \mathcal{L} -jet although the scale (σ) is fixed [46].

The average classification accuracy (%) of K -folds cross-validation test ($K = 10$) for the proposed descriptor is shown in Table V. This table also gives a comparative summary of the results for variants of LBP and other state-of-the-art methods on three well known benchmark texture databases (KTH-TIPS,

Table V: Comparing the average classification accuracy achieved by the proposed approach with those achieved by recent STATE-OF-THE-ART methods

Methods	Classifier	Classification Accuracy (%)		
		KTH-TIPS [50]	Brodatz [53]	CURET [54]
VZ-MR8 [6]	NNC	94.50	94.62	97.43
VZ-Patch [7]	NNC	92.40	87.10	98.03
Lazebnik <i>et al.</i> [17]	NNC	91.30	-	72.50
Zhang <i>et al.</i> [4]	SVM	96.10	-	95.30
MFS [57]	NNC	81.62	-	-
PFS [19]	SVM	97.35	-	-
BIF [5]	Shift NNC	98.50	98.47	98.60
BRINT [35]	NNC	97.75	99.22	97.06
$LBP^{riu2}_{1,8}$ [22]	NNC	82.67	82.16	80.63
DLBP _{3,24} [26]	SVM	86.99	99.16	84.93
$LBP^{sri-su2}_{1,8}$ [31]	NNC	89.73	69.50	85.00
$LBP_{(1,8+2,16+3,24)}$ [22]	NNC	95.17	-	95.84
CLBP_SMC [27]	NNC	97.19	-	97.40
SSLBP [32]	NNC	97.80	-	98.55
Proposed LJP	NNC	98.12	97.31	98.12
Proposed LJP	NSC	99.75	99.16	99.65

Brodatz, and CURET). The following observations have been noted from Table V. The proposed descriptor gives good performance with simple non-parametric NNC classifier on three commonly used challenging databases. The performance is further improved, when an advanced classifier, NSC is used. The NSC classifier gives much better performance compared to the NNC classifier for the same descriptor because: (i) for a given test sample NSC uses all training samples of the same class while NNC uses one training sample only; (ii) NSC is more robust to outlier and noise as it uses the correlation between different samples. DLBP combining with Gabors feature, attains a higher classification rate than original LBP with NNC. However, its performance is quite less than the proposed LJP. This is mainly because DLBP does not consider scale variation, so it can’t provide better performance on complex databases. The scale invariant feature $LBP^{sri-su2}_{R,N}$ provides better performance than $LBP^{riu2}_{R,N}$ where $R = 1, 2, 3$ and $N = 8, 16, 24$, respectively. However the performance is lower than multi-resolution $LBP^{riu2}_{R,N}$ and $CLBP_{S_{R,N}}/M^{riu2}_{R,N}/C$, and much lesser than the proposed descriptor. This happens just because the extraction of consistent and accurate scale for each pixel is difficult. The $LBP^{sri-su2}_{R(i,j),8}$ provides good performance in controlled environment [31], but it fails over more complex databases. Multi-scale BIF [5] at scales $\sigma, 2\sigma, 4\sigma$, and 8σ gives better performance than the proposed LJP with NNC classifier.

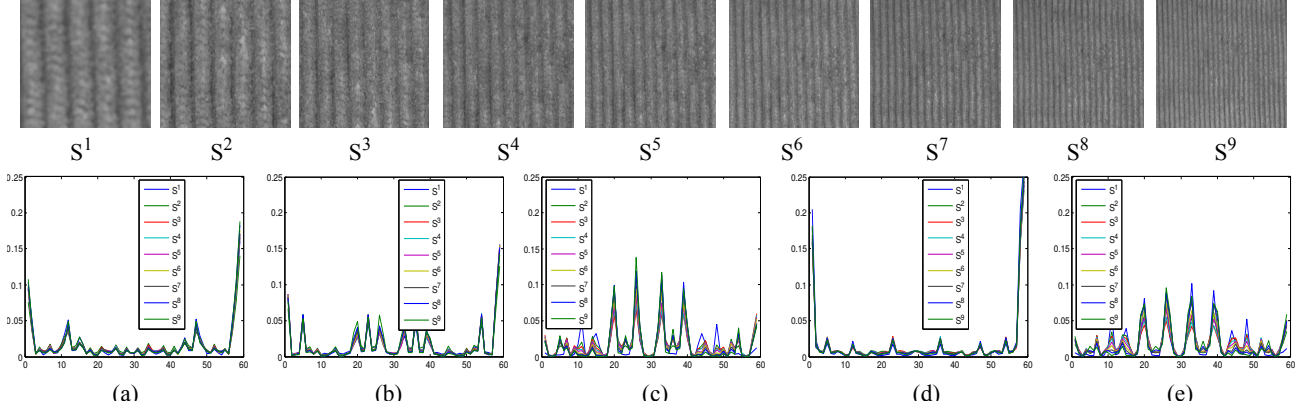


Figure 10: (a)-(e) represent individual histograms $H_{R,N}^l$ of LJP, where $R = 1, N = 8$ and $l \in [2, \mathcal{L}]$ of a texture sample are taken from KTH-TIPS [50] database having 9 different scales where abscissa and ordinate represent number of bins and feature probability distribution, respectively.

This is mainly because BIF uses pyramid histogram with time inefficient shift matching scheme. However, the feature dimension of BIF [5] is too large ($6^4 = 1296$) compared to proposed LJP ($59 \times 6 = 354$) and the shift matching scheme is time consuming. The performance of BIF reduces when scale shifting scheme is not considered [5].

Although the images are captured under scale, rotations, and illumination variations, the proposed LJP gives sound performance in term of mean accuracy and standard deviations i.e. $99.75 \pm 0.790\%$, $99.166 \pm 0.4858\%$, and $99.65 \pm 0.45\%$, on KTH-TIPS [50], Brodatz [53], and CURET [54] texture databases [58], respectively. The classification performance results in Table V shows that the proposed descriptor achieves better and comparable performance compared to the state-of-the-art methods.

Though the trend is clear from the performance Table IV, we have further analysed the performance using one way statistical Analysis of variance (ANOVA) test [59]. ANOVA is a collection of statistical test used to analyze the differences among group means and their associated procedures. The null hypothesis H_0 for the test indicates that, *there is no significant difference among group means*. We have taken the significant level $\alpha = 0.05$ for this ANOVA test. We can reject H_0 if the p -value for an experiment is less than the selected significant level and which implies that the at least one group mean is significantly different from the others. To understand the performance of the proposed LJP descriptor was significantly differs from well-known descriptors such as VZ-Patch, VZ-MR8, BRINT, DLBP, CLBP, and LBP^{riu2} , we conduct an one way ANOVA test with significance level is kept as $\alpha = 0.05$. The test results are shown in Table VI. It is observed from Table VI the p -value ($8.28653e^{-09}$) is less than the pre-select significant level $\alpha = 0.05$ and this indicates that the performance of proposed descriptor significantly differs from other descriptors and hence reject the hypothesis H_0 . In addition, the box plot corresponding to aforementioned ANOVA test is shown in Fig. 11, which also clearly indicates the mean performance of proposed descriptor is significantly better than the well-known descriptors such as VZ-MR8 [6], VZ-Patch [7], BRINT [35], DLBP [26], CLBP [27], and

LBP^{riu2} [22].

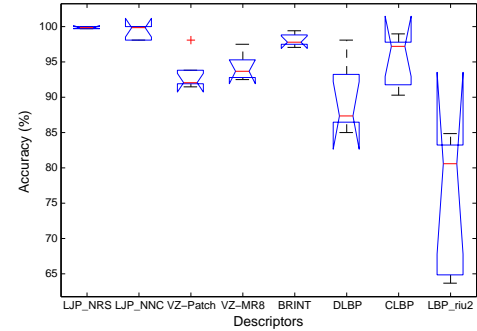


Figure 11: The box plot (Descriptor vs. Accuracy) corresponding to one way statistical ANOVA test for proposed LJP and state-of-the-art descriptors on Outex, KTH-TIPS, Brodatz, CURET databases.

Table VI: One way statistical ANOVA test results for Outex, KTH-TIPS, Brodatz, and CURET databases, where level of significance is selected as $\alpha = 0.05$.

Source	SS	df	MS	F	Prob (p) > F
Groups	2178.22	07	311.175	15.93	$8.28653e^{-09}$
Error	0625.20	32	019.538		
Total	2803.42	39			

D. Experiment #3

To evaluate the performance of the proposed method in noisy environment, the experiments are carried out on Outex_TC10 texture database (discussed in subsec. IV-A) incorporating additive white Gaussian noise with different Signal to Noise Ratio (SNR) in dB. Training and testing scheme is the same as in noise-free situation.

Table VII demonstrates the noise robustness of different methods on Outex_TC10 database by comparing the classification rates for different noise levels (measured using SNR i.e. Signal to Noise Ratio). The proposed descriptor achieves state-of-the-art results in term of mean accuracy and standard deviations $99.95 \pm 0.0976\%$, $99.95 \pm 0.0976\%$, $99.95 \pm 0.0976\%$, $99.95 \pm 0.0976\%$, and $99.83 \pm 0.0975\%$ on SNR

Table VII: Classification Accuracy (%) of Proposed Method and Different STATE-OF-THE-ART Methods on **Outex_TC10** with Different Noise Levels in term of dB.

Methods	Classifier	Classification Accuracy (%)				
		SNR = 100	SNR = 30	SNR = 15	SNR = 10	SNR = 5
LBP ^{1,2} _{R,N} [22]	NNC	95.03	86.93	67.24	49.79	24.06
LBP ^{1,2} _{R,N,k} [55]	NNC	-	99.79	99.76	99.76	99.74
CLBP_SMC [27]	NNC	99.30	98.12	94.58	86.07	51.22
LTP ^{1,2} _{R=3,N=24} [33]	NNC	99.45	98.31	93.44	84.32	57.37
NRLBP ^{1,2} _{R,N} [34]	NNC	84.49	81.16	77.52	70.16	50.88
BRINT [35]	NNC	97.76	96.48	95.47	92.97	88.31
Proposed LJP ^{1,2} _{R,N}	NNC	99.95	99.83	99.79	99.74	99.74
Proposed LJP ^{1,2} _{R,N}	NSC	99.95	99.95	99.95	99.95	99.83

= 100 dB, 30 dB, 15 dB, 10 dB, and 5 dB, respectively. It can be observed that only the proposed LJP method is very modestly improved. This is due to the large smoothing kernels of DtGs which makes it robust to noise. The proposed method has inherited this property from the DtGs in contrast to the LBP and its variants.

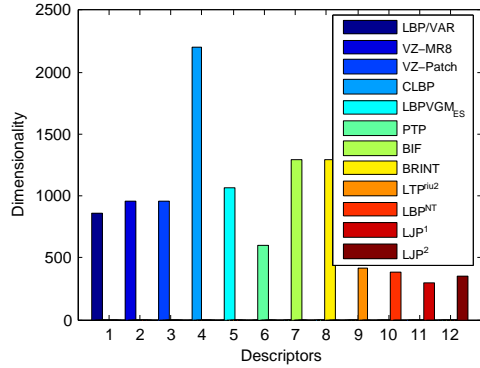


Figure 12: Comparison of feature dimensionality between proposed and state-of-the-art features.

The dimensionality of the proposed descriptors and other state-of-the-art descriptor are shown in Fig. 12. This figure clearly indicates that the dimensionality of the proposed descriptors (LJP¹ has dimensionality of 295 and LJP² has dimensionality 354) are significantly less than the other state-of-the-art methods.

We have implemented the algorithm in MATLAB 2011 environment and executed the program on Intel® Core™2 Duo CPU T6400 @ 2.00GHz × 2 processors and 3GB RAM with UBUNTU 14.04 LTS operating system. The average time to extraction LJP feature for a sample texture image of size (200 × 200) is approximately takes 0.17 seconds. Which shows that LJP descriptor can be applicable in real time scenario.

V. CONCLUSIONS

In this paper, we proposed a simple, efficient yet robust descriptor, LJP for texture classification. First, a jet space representation of a texture image is formed by the responses of a set of derivative of Gaussian (DtGs) filter upto 2nd order where DtGs responses preserves the intrinsic local image structure in a hierarchical way by utilizing the properties of Hermite polynomials. Then the local jet patterns (LJP) are computed by comparing the relation between center and neighboring pixels in the jet space. Finally, the normalized feature

vector is formed by concatenating the histogram of LJP for all elements of jet space representation. The experimental results show that the proposed descriptor provides quite promising performance under scale, rotation, reflection, and illumination variation and fairly robust to the noise. The comparative study indicates the proposed LJP descriptor provides better performance compared to the state-of-the-art methods and in addition, the dimensionality of the final extracted feature vector is significantly less. While offering reasonably less time to extracts feature with a small feature dimension, the proposed descriptor can be applicable in real time scenario. The current work mainly focused on texture classification. In future, the work can be extended on how to exploit LJP descriptor in other domains such as face and object recognition.

ACKNOWLEDGEMENT

The authors sincerely thank Machine Vision Group (MVG), University of Oulu, Finland, Visual Geometry Group (VGG), University of Oxford, UK, Department of Computing, The Hong Kong Polytechnic University, China, and Department of Computer Science, University College London, UK for sharing the source codes of LBP, VZ-MR8, CLBP, and BIF. The authors would also like to thank Manik Varma, Timor Kadir and Andrew Zisserman for providing preprocessed CURET datasets.

REFERENCES

- [1] X. Xie and M. Mirmehdi, "A Galaxy of Texture Features," in *Handbook Of Texture Analysis*. World Scientific, 2008, pp. 375–406.
- [2] R. M. Haralick, K. Shanmugam *et al.*, "Textural features for image classification," *IEEE Transactions on systems, man, and cybernetics*, no. 6, pp. 610–621, 1973.
- [3] T. Randen and J. H. Husoy, "Filtering for texture classification: A comparative study," *IEEE Transactions on pattern analysis and machine intelligence*, vol. 21, no. 4, pp. 291–310, 1999.
- [4] J. Zhang, M. Marszałek, S. Lazebnik, and C. Schmid, "Local features and kernels for classification of texture and object categories: A comprehensive study," *International journal of computer vision*, vol. 73, no. 2, pp. 213–238, 2007.
- [5] M. Crosier and L. D. Griffin, "Using basic image features for texture classification," *International Journal of Computer Vision*, vol. 88, no. 3, pp. 447–460, 2010.
- [6] M. Varma and A. Zisserman, "A statistical approach to texture classification from single images," *International Journal of Computer Vision*, vol. 62, no. 1–2, pp. 61–81, 2005.
- [7] —, "A statistical approach to material classification using image patch exemplars," *IEEE transactions on pattern analysis and machine intelligence*, vol. 31, no. 11, pp. 2032–2047, 2009.
- [8] I. WEISS, "Geometric invariants and object recognition," *International journal of computer vision*, vol. 10, no. 3, pp. 207–231, 1993.
- [9] R. L. Kashyap and A. Khotanzad, "A model-based method for rotation invariant texture classification," *IEEE Transactions on Pattern Analysis and Machine Intelligence*, no. 4, pp. 472–481, 1986.
- [10] J. Mao and A. K. Jain, "Texture classification and segmentation using multiresolution simultaneous autoregressive models," *Pattern recognition*, vol. 25, no. 2, pp. 173–188, 1992.
- [11] J.-L. Chen and A. Kundu, "Rotation and gray scale transform invariant texture identification using wavelet decomposition and hidden Markov model," *IEEE Transactions on Pattern Analysis and Machine Intelligence*, vol. 16, no. 2, pp. 208–214, 1994.
- [12] H. Deng and D. A. Clausi, "Gaussian MRF rotation-invariant features for image classification," *IEEE transactions on pattern analysis and machine intelligence*, vol. 26, no. 7, pp. 951–955, 2004.
- [13] B. B. Chaudhuri and N. Sarkar, "Texture segmentation using fractal dimension," *IEEE Transactions on Pattern Analysis and Machine Intelligence*, vol. 17, no. 1, pp. 72–77, 1995.

- [14] M. Varma and R. Garg, "Locally invariant fractal features for statistical texture classification," in *Computer Vision, 2007. ICCV 2007. IEEE 11th International Conference on*. IEEE, 2007, pp. 1–8.
- [15] L. Liu and P. Fieguth, "Texture classification from random features," *IEEE Transactions on Pattern Analysis and Machine Intelligence*, vol. 34, no. 3, pp. 574–586, 2012.
- [16] C.-H. Yao and S.-Y. Chen, "Retrieval of translated, rotated and scaled color textures," *Pattern Recognition*, vol. 36, no. 4, pp. 913–929, 2003.
- [17] S. Lazebnik, C. Schmid, and J. Ponce, "A sparse texture representation using local affine regions," *IEEE Transactions on Pattern Analysis and Machine Intelligence*, vol. 27, no. 8, pp. 1265–1278, 2005.
- [18] Y. Xu, H. Ji, and C. Fermüller, "Viewpoint invariant texture description using fractal analysis," *International Journal of Computer Vision*, vol. 83, no. 1, pp. 85–100, 2009.
- [19] Y. Quan, Y. Xu, and Y. Sun, "A distinct and compact texture descriptor," *Image and Vision Computing*, vol. 32, no. 4, pp. 250–259, 2014.
- [20] J. Zhang, J. Liang, and H. Zhao, "Local energy pattern for texture classification using self-adaptive quantization thresholds," *IEEE transactions on image processing*, vol. 22, no. 1, pp. 31–42, 2013.
- [21] T. Ojala, M. Pietikäinen, and D. Harwood, "A comparative study of texture measures with classification based on featured distributions," *Pattern recognition*, vol. 29, no. 1, pp. 51–59, 1996.
- [22] T. Ojala, M. Pietikäinen, and T. Maenpää, "Multiresolution gray-scale and rotation invariant texture classification with local binary patterns," *IEEE Transactions on pattern analysis and machine intelligence*, vol. 24, no. 7, pp. 971–987, 2002.
- [23] M. Heikkilä, M. Pietikäinen, and C. Schmid, "Description of interest regions with local binary patterns," *Pattern recognition*, vol. 42, no. 3, pp. 425–436, 2009.
- [24] B. Zhang, Y. Gao, S. Zhao, and J. Liu, "Local derivative pattern versus local binary pattern: face recognition with high-order local pattern descriptor," *IEEE transactions on image processing*, vol. 19, no. 2, pp. 533–544, 2010.
- [25] Z. Guo, L. Zhang, and D. Zhang, "Rotation invariant texture classification using LBP variance (LBPV) with global matching," *Pattern recognition*, vol. 43, no. 3, pp. 706–719, 2010.
- [26] S. Liao, M. W. Law, and A. C. Chung, "Dominant local binary patterns for texture classification," *IEEE transactions on image processing*, vol. 18, no. 5, pp. 1107–1118, 2009.
- [27] Z. Guo, L. Zhang, and D. Zhang, "A completed modeling of local binary pattern operator for texture classification," *IEEE Transactions on Image Processing*, vol. 19, no. 6, pp. 1657–1663, 2010.
- [28] S. R. Dubey, S. K. Singh, and R. K. Singh, "Rotation and illumination invariant interleaved intensity order-based local descriptor," *IEEE Transactions on Image Processing*, vol. 23, no. 12, pp. 5323–5333, 2014.
- [29] —, "Local wavelet pattern: A new feature descriptor for image retrieval in medical ct databases," *IEEE Transactions on Image Processing*, vol. 24, no. 12, pp. 5892–5903, 2015.
- [30] —, "Multichannel decoded local binary patterns for content-based image retrieval," *IEEE Transactions on Image Processing*, vol. 25, no. 9, pp. 4018–4032, 2016.
- [31] Z. Li, G. Liu, Y. Yang, and J. You, "Scale-and rotation-invariant local binary pattern using scale-adaptive texton and subuniform-based circular shift," *IEEE Transactions on Image Processing*, vol. 21, no. 4, pp. 2130–2140, 2012.
- [32] Z. Guo, X. Wang, J. Zhou, and J. You, "Robust texture image representation by scale selective local binary patterns," *IEEE Transactions on Image Processing*, vol. 25, no. 2, pp. 687–699, 2016.
- [33] X. Tan and B. Triggs, "Enhanced local texture feature sets for face recognition under difficult lighting conditions," in *International Workshop on Analysis and Modeling of Faces and Gestures*. Springer, 2007, pp. 168–182.
- [34] J. Ren, X. Jiang, and J. Yuan, "Noise-resistant local binary pattern with an embedded error-correction mechanism," *IEEE Transactions on Image Processing*, vol. 22, no. 10, pp. 4049–4060, 2013.
- [35] L. Liu, Y. Long, P. W. Fieguth, S. Lao, and G. Zhao, "Brint: binary rotation invariant and noise tolerant texture classification," *IEEE Transactions on Image Processing*, vol. 23, no. 7, pp. 3071–3084, 2014.
- [36] L. Florack, B. T. H. Romeny, M. Viergever, and J. Koenderink, "The Gaussian scale-space paradigm and the multiscale local jet," *International Journal of Computer Vision*, vol. 18, no. 1, pp. 61–75, 1996.
- [37] A. P. Witkin, "Scale-Space filtering," in *Proceedings of the Eighth international joint conference on Artificial intelligence-Volume 2*. Morgan Kaufmann Publishers Inc., 1983, pp. 1019–1022.
- [38] T. Lindeberg, *Scale-Space theory in computer vision*. Springer Science & Business Media, 1994, vol. 256.
- [39] —, "Scale-space theory: A basic tool for analyzing structures at different scales," *Journal of applied statistics*, vol. 21, no. 1-2, pp. 225–270, 1994.
- [40] J. J. Koenderink, "The structure of images," *Biological cybernetics*, vol. 50, no. 5, pp. 363–370, 1984.
- [41] D. G. Lowe, "Distinctive image features from scale-invariant keypoints," *International journal of computer vision*, vol. 60, no. 2, pp. 91–110, 2004.
- [42] L. D. Griffin and M. Lillholm, "Symmetry sensitivities of derivative-of-gaussian filters," *IEEE transactions on pattern analysis and machine intelligence*, vol. 32, no. 6, pp. 1072–1083, 2010.
- [43] J. D. Victor and B. W. Knight, "Simultaneously band and space limited functions in two dimensions, and receptive fields of visual neurons," in *Perspectives and Problems in Nonlinear Science*. Springer, 1994, pp. 375–419.
- [44] R. A. Young, R. M. Lesperance, and W. W. Meyer, "The gaussian derivative model for spatial-temporal vision: I. cortical model," *Spatial vision*, vol. 14, no. 3, pp. 261–319, 2001.
- [45] J.-B. Martens, "The hermite transform-theory," *IEEE Transactions on Acoustics, Speech, and Signal Processing*, vol. 38, no. 9, pp. 1595–1606, 1990.
- [46] J. J. Koenderink and A. J. van Doorn, "Representation of local geometry in the visual system," *Biological cybernetics*, vol. 55, no. 6, pp. 367–375, 1987.
- [47] L. D. Griffin, "The second order local-image-structure solid," *IEEE Transactions on Pattern Analysis and Machine Intelligence*, vol. 29, no. 8, pp. 1355–1366, 2007.
- [48] J. J. Koenderink and A. J. van Doorn, "Generic neighborhood operators," *IEEE Transactions on Pattern Analysis and Machine Intelligence*, vol. 14, no. 6, pp. 597–605, 1992.
- [49] L. D. Griffin and M. Lillholm, "Image features and the 1-D, 2nd order Gaussian derivative jet," in *International Conference on Scale-Space Theories in Computer Vision*. Springer, 2005, pp. 26–37.
- [50] E. Hayman, B. Caputo, M. Fritz, and J.-O. Eklundh, "On the significance of real-world conditions for material classification," in *European conference on computer vision*. Springer, 2004, pp. 253–266.
- [51] J. Wright, A. Y. Yang, A. Ganesh, S. S. Sastry, and Y. Ma, "Robust face recognition via sparse representation," *IEEE transactions on pattern analysis and machine intelligence*, vol. 31, no. 2, pp. 210–227, 2009.
- [52] T. Ojala, T. Maenpää, M. Pietikäinen, J. Viertola, J. Kyllönen, and S. Huovinen, "Outex-new framework for empirical evaluation of texture analysis algorithms," in *Pattern Recognition, 2002. Proceedings. 16th International Conference on*, vol. 1. IEEE, 2002, pp. 701–706.
- [53] P. Brodatz, *Textures: a photographic album for artists and designers*. New York, NY, USA: Dover Pubns, 1966.
- [54] K. J. Dana, B. Van Ginneken, S. K. Nayar, and J. J. Koenderink, "Reflectance and texture of real-world surfaces," *ACM Transactions On Graphics (TOG)*, vol. 18, no. 1, pp. 1–34, 1999.
- [55] A. Fathi and A. R. Naghsh-Nilchi, "Noise tolerant local binary pattern operator for efficient texture analysis," *Pattern Recognition Letters*, vol. 33, no. 9, pp. 1093–1100, 2012.
- [56] K. Wang, C.-E. Bichot, C. Zhu, and B. Li, "Pixel to patch sampling structure and local neighboring intensity relationship patterns for texture classification," *IEEE Signal Processing Letters*, vol. 20, no. 9, pp. 853–856, 2013.
- [57] Y. Xu, H. Ji, and C. Fermüller, "A projective invariant for textures," in *Computer Vision and Pattern Recognition, 2006 IEEE Computer Society Conference on*, vol. 2. IEEE, 2006, pp. 1932–1939.
- [58] K. Mikolajczyk and C. Schmid, "A performance evaluation of local descriptors," *IEEE transactions on pattern analysis and machine intelligence*, vol. 27, no. 10, pp. 1615–1630, 2005.
- [59] G. R. Iversen and H. Norpoth, *Analysis of variance*. Sage, 1987, no. 1.